Structural insights into FTO's catalytic mechanism for the demethylation of multiple RNA substrates

Xiao Zhang[a,1], Lian-Huan Wei[a,1], Yuxin Wang[b,1], Yu Xiao[a,1], Jun Liu[a], Wei Zhang[a], Ning Yan[c], Gubu Amu[c], Xinjing Tang[c], Liang Zhang[b,2], and Guifang Jia[a,d,2]

[a]Synthetic and Functional Biomolecules Center, Beijing National Laboratory for Molecular Sciences, Key Laboratory of Bioorganic Chemistry and Molecular Engineering of Ministry of Education, College of Chemistry and Molecular Engineering, Peking University, Beijing 100871, China; [b]Department of Pharmacology and Chemical Biology, Shanghai Jiao Tong University School of Medicine, Shanghai 200025, China; [c]State Key Laboratory of Natural and Biomimetic Drugs, School of Pharmaceutical Sciences, Peking University, Beijing 100191, China; and [d]Beijing Advanced Innovation Center for Genomics, Peking University, Beijing 100871, China

Edited by Rupert G. Fray, University of Nottingham, Loughborough, United Kingdom, and accepted by Editorial Board Member Caroline Dean January 3, 2019 (received for review December 8, 2018)

FTO demethylates internal N^6-methyladenosine (m^6A) and N^6,2′-*O*-dimethyladenosine (m^6A_m; at the cap +1 position) in mRNA, m^6A and m^6A_m in snRNA, and N^1-methyladenosine (m^1A) in tRNA in vivo, and in vitro evidence supports that it can also demethylate N^6-methyldeoxyadenosine (6mA), 3-methylthymine (3mT), and 3-methyluracil (m^3U). However, it remains unclear how FTO variously recognizes and catalyzes these diverse substrates. Here we demonstrate—in vitro and in vivo—that FTO has extensive demethylation enzymatic activity on both internal m^6A and cap m^6A_m. Considering that 6mA, m^6A, and m^6A_m all share the same nucleobase, we present a crystal structure of human FTO bound to 6mA-modified ssDNA, revealing the molecular basis of the catalytic demethylation of FTO toward multiple RNA substrates. We discovered that (*i*) N^6-methyladenine is the most favorable nucleobase substrate of FTO, (*ii*) FTO displays the same demethylation activity toward internal m^6A and m^6A_m in the same RNA sequence, suggesting that the substrate specificity of FTO primarily results from the interaction of residues in the catalytic pocket with the nucleobase (rather than the ribose ring), and (*iii*) the sequence and the tertiary structure of RNA can affect the catalytic activity of FTO. Our findings provide a structural basis for understanding the catalytic mechanism through which FTO demethylates its multiple substrates and pave the way forward for the structure-guided design of selective chemicals for functional studies and potential therapeutic applications.

RNA modification | RNA demethylase | FTO | enzyme catalysis | structure

The *FTO* gene was originally cloned in a study of a fused-toe mutant mouse and named Fatso (FTO); its function was unknown (1). It was renamed the fat mass and obesity-associated (*FTO*) gene after genome-wide associated studies linked it with human obesity (2, 3). A human obesity-related function was further substantiated by phenotypes observed in *FTO* knockout and overexpression mouse models (4, 5). Genetic variants in the *FTO* gene are also associated with cancers (6, 7), metabolic disorders (8, 9), and neurological diseases (10, 11). These intriguing phenotypes and genetic functions attracted tremendous research interest in the molecular mechanisms and physiological substrate(s) of FTO.

FTO was identified as a homolog of the Fe(II)/α-ketoglutarate acid (α-KG)–dependent AlkB family dioxygenases and was first reported to catalytically demethylate 3-methylthymine (3mT) in ssDNA and 3-methyluracil (m^3U) in ssRNA (12, 13). The crystal structure of FTO provided valuable information about the composition and conformation of the enzyme catalytic pocket and activity (14). Later on, FTO was identified as the first RNA demethylase that catalyzes oxidative demethylation of N^6-methyladenosine (m^6A) on mRNA in vitro and in vivo (15, 16). This discovery stimulated extensive worldwide research efforts in recent years into dynamic m^6A and other RNA modifications in biological regulation (17–25). FTO-mediated m^6A demethylation has been found to regulate many biological processes, including preadipocyte differentiation (22), heat shock stress-induced cap-independent translation (23), UV-induced DNA damage (24), and acute myeloid leukemia (25). N^6,2′-*O*-dimethyladenosine (m^6A_m)—a distinct form of m^6A with a 2′-*O*-methylation at the ribose ring—is a substrate of FTO in vitro (26). It has long been known that m^6A_m marks exist predominantly at the +1 position following the N^7-methylguanosine (m^7G) cap at the 5′ terminus of mRNA molecules (henceforth termed cap m^6A_m). The m^6A distribution along mRNA, as mapped by N^6-methyladenosine sequencing, found a distinct peak immediately following the transcription start site (27), which in fact represents cap-associated m^6A_m, considering that the m^6A antibody recognizes both m^6A and m^6A_m. m^6A individual-nucleotide-resolution cross-linking and immunoprecipitation identified certain mRNAs containing cap m^6A_m (28). Cap m^6A_m marks occur much less frequently than internal m^6A marks; for instance, mRNA from H1-ESC cells had 33-fold more internal m^6A than cap m^6A_m (29).

Significance

The RNA modification N^6-methyladenosine (m^6A) was the first physiological substrate of FTO to be discovered. Recently, cap N^6,2′-*O*-dimethyladenosine (m^6A_m), internal m^6A_m, and N^1-methyladenosine were also found to be physiological substrates of FTO. However, the catalytic mechanism through which FTO demethylates its multiple RNA substrates remains largely mysterious. Here we present the first structure of FTO bound to N^6-methyldeoxyadenosine–modified ssDNA. We show that N^6-methyladenine is the most favorable nucleobase substrate of FTO and that the sequence and the tertiary structure of RNA can affect the catalytic activity of FTO. Our findings provide a structural basis for understanding FTO's catalytic mechanism for the demethylation of multiple RNA substrates and shed light on the mechanism through which FTO is involved in diseases or biological processes.

Author contributions: X.Z., L.-H.W., J.L., and G.J. designed research; X.Z., L.-H.W., Y.X., J.L., and W.Z. performed research; Y.W., N.Y., G.A., X.T., and L.Z. contributed new reagents/analytic tools; X.Z., L.-H.W., Y.W., Y.X., L.Z., and G.J. analyzed data; and X.Z., L.Z., and G.J. wrote the paper.

The authors declare no conflict of interest.

This article is a PNAS Direct Submission. R.G.F. is a guest editor invited by the Editorial Board.

Data deposition: The atomic coordinates and structure factors have been deposited in the Protein Data Bank, www.wwpdb.org (PDB ID code 5ZMD).

[1]X.Z., L.-H.W., Y.W., and Y.X. contributed equally to this work.

[2]To whom correspondence may be addressed. Email: liangzhang2014@sjtu.edu.cn or guifangjia@pku.edu.cn.

This article contains supporting information online at www.pnas.org/lookup/suppl/doi:10.1073/pnas.1820574116/-/DCSupplemental.

Published online February 4, 2019.

In 2017, Mauer et al. (30) proposed that FTO mediates cap m^6A_m demethylation and shows almost no demethylation activity on internal m^6A in cells, a conclusion that diametrically opposes numerous previous findings (15, 21–25). A recent finding characterized the cap m^6A_m writer (CAPAM) and reported that *CAPAM* knockout cells grow well and show a similar growth rate than wild-type cells (31), which is different from the phenotypic features of *FTO* knockdown cells (22, 25) and indicates the cap m^6A_m is not the major substrate of FTO for its phenotypes and genetic functions. Recently published results systematically identified the in vivo substrates of FTO, including m^6A and cap m^6A_m in mRNA, m^6A and m^6A_m in snRNA, and m^1A in tRNA, and thereby revealed that the subcellular localization of FTO affects its ability to perform different RNA modifications (32). However, the molecular mechanism for the enzymatic demethylation of FTO toward multiple RNA substrates remains unclear.

In this study, our in vitro and in vivo biochemical results conclusively establish that FTO demethylates both internal m^6A and cap m^6A_m marks in mRNA. Given the considerable challenges of crystallizing FTO in a complex with nucleic acids, we rationally designed double mutations outside of FTO's catalytic pocket and thus successfully obtained the structure of human FTO bound to N^6-methyldeoxyadenosine–modified ssDNA (FTO-6mA). We investigated the recognition modes of multiple RNA substrates in FTO's catalytic pocket and investigated which nucleobase is the most energetically favorable for binding with FTO; 6mA, m^6A, and m^6A_m share the same recognition mode in FTO's catalytic pocket, except for structural differences of the ribose ring. We explored whether the structural differences of the ribose ring may affect the demethylation activities of FTO when internal m^6A and m^6A_m are positioned in the same RNA sequence and further investigated how FTO binds RNA and tested whether the sequence and the structure of RNA affect FTO's activity. Our results demonstrate that N^6-methyladenine is the favored nucleobase for FTO and find that FTO exhibits the same demethylation activity toward internal m^6A and m^6A_m positioned in the same RNA sequence. Our work also shows that the sequence and the tertiary structure of RNA affect the demethylation activity of FTO.

Results

FTO Mediates Extensive Demethylation of Internal m^6A and Cap m^6A_m in Vitro and in Vivo. Mauer et al. (30) proposed that cap m^6A_m and not m^6A is the cellular physiological substrate of FTO, which diametrically opposes most previous findings (15, 21–25). Seeking to resolve this apparent discrepancy and to further characterize the physiological substrate of FTO, we investigated the demethylation functions of FTO with biologically relevant substrates in vitro and in vivo. Here we used an mRNA digestion procedure which allowed us to simultaneously detect both internal m^6A and cap m^6A_m marks and to measure the ratios of m^6A to A (m^6A/A) and m^6A_m to A (m^6A_m/A) using quantitative ultraperformance liquid chromatography coupled with tandem mass spectrometry (UPLC-MS/MS).

We first performed in vitro demethylation assays with recombinant FTO (*SI Appendix*, Fig. S1) and mRNA isolated from HeLa cells. This analysis showed that the total amount of m^6A was ∼10-fold larger than the amount of cap m^6A_m in HeLa mRNAs, and FTO (1 μM in 50 μL) demethylated nearly all of the cap m^6A_m (>99%) and 80% of the internal m^6A in 400 ng of mRNA (Fig. 1*A* and *SI Appendix*, Fig. S2*A*). We lowered the FTO concentration to achieve incomplete demethylation of cap m^6A_m to estimate the in vitro catalytic efficiency of FTO for m^6A and for cap m^6A_m. We observed that 0.08 μM of FTO (50 μL) demethylated 86% of cap m^6A_m and 12% of internal m^6A in 400 ng of isolated mRNA (Fig. 1*B* and *SI Appendix*, Fig. S2*B*). Note that the total amount of m^6A was ∼10-fold larger than the amount of cap m^6A_m in mRNAs; the absolute number of m^6A bases (0.245 per 1,000 A bases) reversed

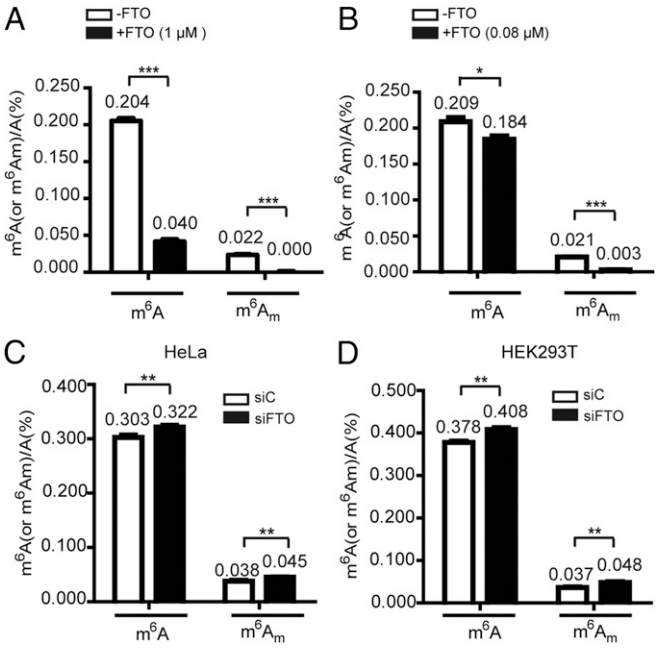

Fig. 1. FTO demethylates both internal m^6A and cap m^6A_m in vitro and in vivo. (*A* and *B*) UPLC-MS/MS quantification of internal m^6A/A and cap m^6A_m/A ratios in mRNA treated with FTO protein in vitro. Here 400 ng of purified mRNA from HeLa cells were treated with 1 μM of FTO (*A*) or 0.08 μM of FTO (*B*) under standard demethylation conditions in 50 μL of reaction mixture for 1 h at 37 °C. (*C* and *D*) UPLC-MS/MS quantification of internal m^6A/A and cap m^6A_m/A ratios in mRNA isolated from HeLa (*C*) and HEK293T (*D*) cells with or without *FTO* knockdown. Error bars indicate the mean ± SEM ($n = 6$, three biological replicates × two technical replicates), determined using an unpaired Student's *t* test. $^*P < 0.05$; $^{**}P < 0.01$; $^{***}P < 0.001$.

by FTO (0.08 μM in 50 μL) is ∼1.3-fold more than that of m^6A_m (0.178 per 1,000 A bases) (*SI Appendix*, Fig. S3*A*). We next examined the in vivo demethylation performance of FTO by performing siRNA knockdown assays in HeLa and HEK293T cells (*SI Appendix*, Fig. S4). Upon *FTO* knockdown in HeLa cells, FTO demethylates 0.185 m^6A and 0.071 cap m^6A_m molecules per 1,000 A bases (Fig. 1*C* and *SI Appendix*, Fig. S3*B*). Consistently, a similar result was also observed in HEK293T cells (Fig. 1*D* and *SI Appendix*, Fig. S3*C*). Collectively, these results confirm that FTO can demethylate both internal m^6A and cap m^6A_m in vitro and in vivo. During the revision of this paper, Wei et al. (32) reported that FTO can demethylate both m^6A and cap m^6A_m in vitro and in cells, which is consistent with our results.

Rational Design of FTO Mutations Facilities Crystallization of FTO–Oligonucleotide Complex. To elucidate how FTO recognizes and demethylates its physiological substrates, we decided to crystallize an FTO–oligonucleotide complex. However, we had a hard time obtaining crystals of an FTO–ssRNA complex for X-ray diffraction. This was not surprising, as crystallization of the AlkB family protein–nucleic acid complexes is known to be challenging due to the weak binding of these proteins with nucleic acids (33). Two strategies have been successfully used to overcome the difficulty: chemical bisulfide cross-linking and active-site mutation (34, 35). Here we chose to engineer FTO with site-directed mutagenesis to increase the binding ability of FTO to nucleic acids. The enzymatic activity of AlkB family proteins mainly depends on the recognition of a methylated nucleobase in the catalytic pocket (34). Considering that 6mA, m^6A, and m^6A_m share the same nucleobase, we crystallized the complex of FTO bound to 6mA-modified

ssDNA to characterize FTO's catalytic mechanism for the demethylation of multiple RNA substrates.

We generated FTO variants with site-directed mutations; these were subsequently searched for variants that (*i*) exhibit increased binding affinity for 6mA-modified oligo but (*ii*) do not alter the enzyme's demethylation activity. Superimposition of the *apo* FTO structure with a structure of an AlkB-1mA (N^1-methyladenine) modified ssDNA complex led us to select five amino acids—inside and outside of the FTO catalytic pocket—for rational mutation (E234A, R96A, Y106F, Q86K, and Q306K) (*SI Appendix*, Fig. S5*A*). We then separately expressed and purified wild-type FTO (termed as FTO^{WT}) and these FTO mutants from *E. coli* (*SI Appendix*, Fig. S1) and determined their binding affinities (equilibrium binding constants) with fluorescein-labeled 6mA-modified ssDNA using fluorescence anisotropy measurements (36). The Q86K and Q306K mutations increased the binding affinity of FTO to ssDNA by, respectively, ∼1.5-fold and ∼10-fold, while R96A and Y106F both decreased binding affinity by approximately twofold; the E234A mutation did not significantly affect binding affinity (*SI Appendix*, Figs. S5*B* and S6). We then generated a Q86K/Q306K double-mutation FTO variant (termed as $FTO^{Q86K/Q306K}$) and found this variant had an ∼16-fold increase in binding affinity over FTO^{WT} ($K_d = 0.23$ μM). We further confirmed that $FTO^{Q86K/Q306K}$ does not obviously alter the m^6A demethylation activity (*SI Appendix*, Fig. S5*C*), which makes sense given that the Q86K/Q306K mutations are in the oligonucleotide binding motif of FTO, not in its catalytic pocket (*SI Appendix*, Fig. S5*A*).

The Structure of FTO Bound to 6mA-Modified ssDNA Reveals a Specific Substrate Binding and Catalytic Mechanism. Our strategy of increasing the FTO substrate binding affinity facilitated the crystallization of $FTO^{Q86K/Q306K}$ bound to 6mA-modified 10-mer ssDNA (Fig. 2*A*). Needlelike crystals appeared within 1 wk. However, the diffraction of these crystals showed an obvious anisotropy property with two directions (*b* and *c*) diffracting to 3.0 and 3.1 Å but the other direction (*a*) diffracting to only 3.7 Å (*SI Appendix*, Fig. S7). We finally scaled the overall resolution to 3.3 Å, optimized the data, and solved the structure by molecular replacement using the published *apo* FTO structure [Protein Data Bank (PDB) ID code 3LFM] (14) (*SI Appendix*, *Supplementary Text* and Table S1). Notably, we found that most of the nucleotides (except the first one at the 5′ terminus) in the structure, especially 6mA, are well fitted into the electron density, although the resolution is low (*SI Appendix*, Fig. S8).

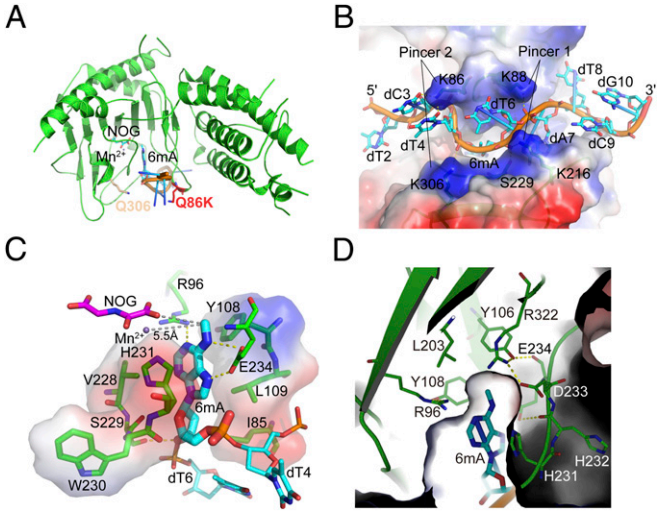

Fig. 2. Crystal structure of FTO bound to 6mA-modified ssDNA. (*A*) The Q86K and Q306K double-mutation sites of FTO in the structure. (*B*) Overall structure of FTO-6mA. The electrostatic surface of FTO and sticks of ssDNA were generated by PyMOL. The color range from red (negative) to blue (positive) represents the surface electrostatic potentials of −73.5 to +73.5 e/kT. ssDNA is colored in cyan. (*C*) Detailed interactions in the catalytic pocket of FTO to accommodate 6mA. The gray dashes represent the distance between the N^6-methyl group with NOG and Mn^{2+}. The electrostatic surface of the residues involved in hydrophobic interactions with 6mA is shown. (*D*) The hydrophobic cave around the N^6-methyl group of 6mA. Residues involved in the interactions are shown and labeled.

The asymmetric crystallographic unit contains four FTO–ssDNA complexes, in which every two FTO molecules stack two ssDNA strands under the same 5′ to 3′ direction (*SI Appendix*, Fig. S9). Within the complex, two pairs of positively charged residues from two critical loops near the oligonucleotides binding area of FTO contribute most of the hydrophilic interactions with the oligonucleotide. They hold the oligonucleotide like two pairs of pincers and bend it into an M shape (Fig. 2*B*). The first pincer (pincer 1) consists of two lysine residues: K88 and K216. K88 is located on a short loop (residues 86–88) between β2 and β3, while K216 is within a long loop (residues 210–223, henceforth called the FTO unique loop) between β7 and β8; FTO is the only human AlkB family member that contains this type of loop (*SI Appendix*, Fig. S10). K88 and K216 stabilize the ssDNA through hydrogen bonds (H bonds) between their side chains and the phosphates of, respectively, A7 and T6 of the ssDNA molecule; these bonds effectively twist the strand ∼45° as a result of steric hindrances with the side chains.

The second pincer (pincer 2) consists of two mutated lysine residues: K86 and K306 (glutamines in FTO^{WT}) (Fig. 2*B*). K86 (Q86 in FTO^{WT}) is located on the short loop between β2 and β3 next to K88, and its side chain forms strong hydrophilic interactions with the O2 atom of the pyrimidine rings of C3 and T4 in the ssDNA; given this interaction, it is likely that residues at this position contribute strongly to substrate sequence recognition and stabilization. In contrast, K306 (Q306 in FTO^{WT}) is located on β13 and has a hydrophilic interaction with the phosphate backbone of 6mA. These side chain–base interactions significantly increase the binding affinity of $FTO^{Q86K/Q306K}$ to ssDNA compared with FTO^{WT}, which is consistent with the observations from the fluorescence anisotropy measurements (*SI Appendix*, Figs. S5*B* and S6). Moreover, whereas the nucleic acid binding tunnel of pincer 1 is narrow, the distance between the two residues (K86 and K306) of pincer 2 is significant longer (11.2 Å), generating a flat and large space next to pincer 2 that potentially accommodates tertiary structured RNAs like stem loops as substrates (*SI Appendix*, Fig. S11*A*). Additionally, the 5′ and 3′ ends of the 10-mer ssDNA have few interactions with FTO (*SI Appendix*, *Supplementary Text* and Fig. S12).

Inside the catalytic pocket, the purine ring of 6mA is stacked between Y108, L109, V228, and H231, and the deoxyribose ring is stacked between I85, V228, S229, W230, and H231 through hydrophobic interactions (Fig. 2*C*). The N1 atom on the 6mA purine ring interacts with R96 via a H bond, while the N6 and N7 atoms form H bonds with E234, thereby locking the base in place. Note that the N^6-methyl group is stabilized in a hydrophobic pocket formed by the side chains of R96, Y106, Y108, L203, and R322 (Fig. 2*D*) and is orientated to Fe(II) and α-KG for oxidation (Fig. 2*C*). These residues form a stable H bond network with each other, making the pocket stable and robust. These structural insights help explain the aforementioned biochemical results that the R96A and Y106F mutations significantly reduced the binding affinity: each mutation would disrupt the H bond network and reduce the stability of the hydrophobic pocket used for holding the N^6-methyl group of 6mA (*SI Appendix*, Figs. S5*B* and S6).

Structural-based sequence alignment among AlkB family members shows that most of the residues involved in hydrophobic

interactions with substrate bases are conserved (such as Y108, L109, and H231 in FTO), suggesting that these residues strongly contribute to base stabilization across the entire protein family (Fig. 2 *C* and *D* and *SI Appendix*, Fig. S10). However, given the extensive variation among the family members of the residues involved in hydrophilic interactions with substrate bases, it seems clear that the R96 and E234 residues of FTO are responsible for specific substrate base recognition (*SI Appendix*, Fig. S10). In addition, cofactors Mn^{2+} [which occupies the Fe(II)-binding site but does not support catalysis] and α-KG analog *N*-oxalylglycine (NOG) molecules are stabilized in the FTO catalytic pocket predominantly through H bonds (N205, D233, Y295, H307, R316, S318, and R322) and coordinate bonds (H231, D233, and H307) (*SI Appendix*, Figs. S10 and S11*B*), indicating a highly conserved catalytic mechanism among the AlkB family members.

FTO Exhibits a Preference for the Nucleobase N^6-Methyladenine over Its Other Reported Substrates. In vivo and in vitro evidence has established that FTO demethylates multiple methylated modifications (12, 13, 15, 30, 32), yet it is not known how FTO recognizes multiple substrates in the catalytic pocket or for which substrates FTO exhibits the highest affinity. Thus, we further structurally elucidate the catalytic mechanisms using the computational superimposition strategy.

The superposition of the FTO-3mT nucleoside structure (PDB ID code 3LFM) (14) into the FTO-6mA structure indicates high similarity (rmsd = 0.615); most of the key residues inside the catalytic pocket adopt a similar conformation, except E234 (Fig. 3*A*). The side chain of E234 forms H bonds with the N6 and N7 atoms of the 6mA purine ring for base stabilization; however, the amide nitrogen of E234 in the FTO-3mT complex forms only a weak H bond with the O4 atom of 3mT. Moreover, the side chain of E234 is pushed toward the outside of the catalytic pocket (~70°) by the 3-methyl group of 3mT during the ~45° counterclockwise rotation of 3mT, causing an unfavorable and unstable conformation of 3mT in the catalytic pocket, which obviously weakens the catalytic activity of FTO on 3mT (13, 14). As expected, the E234A FTO mutant variant showed a threefold increase in enzymatic activity toward 3mT. In contrast, this variant had only a 10% increase in the m^6A demethylation activity (Fig. 3*B*). Recall that this mutation did not interfere with oligonucleotide substrate binding (*SI Appendix*, Figs. S5*B* and S6), suggesting that E234 functions in nucleobase selection and recognition inside the catalytic pocket.

We next investigated the catalytic mechanism through which FTO recognizes m^6A and m^6A_m in the catalytic pocket by examining the superposition of these two nucleosides into the FTO-6mA structure (Fig. 3*C*). As three confirmed FTO substrates share the same nucleobase (N^6-methyladenine), any difference in recognition could be assumed to result from some influence of differences at the 2′ position of the ribose ring of these substrates (Fig. 3*C*). The 2′ position of the deoxyribose ring of 6mA points toward a small cave composed of residues V228 and S229 and nucleotide A7, and the side chain of S229 forms a H bond with the oxygen atom on the phosphate of T6, holding the oligonucleotide in place for catalysis (Fig. 2*C*).

The superposition of the m^6A nucleoside into the FTO-6mA structure shows that the additional hydroxyl group (2′OH) of m^6A on the 2′ position of the ribose ring further points toward the same cave. Although the distance between 2′OH and the side chain of S229 in the structure is likely too far to enable formation of a H bond (4.2 Å), it is possible that the insertion of the 2′OH induces an ~15° rotation of the S229 side chain, which could potentiate the formation of a weak H bond for further stabilization of the m^6A nucleoside (Fig. 3*C* and *SI Appendix*, Fig. S13). In contrast, the methoxy group on the 2′ position of the ribose ring of m^6A_m could be reasonably expected to insert further into this small cave. Thus, either the spatial configuration or the hydrophobic properties of the cave apparently accommodate and stabilize the 2′-OMe of m^6A_m; however, m^6A_m might lose the potential hydrophilic interaction between the 2′OH and S229 due to the methylation of the hydroxyl group, causing lower activity in catalyzing m^6A_m compared with m^6A.

To determine whether the structural difference in the ribose ring of m^6A and m^6A_m affects the enzymatic activity of FTO, we performed demethylation assays with a purified protein (either FTO^{WT} or FTO^{S229A}) and a synthetic 15-mer RNA (Oligo3) containing either m^6A or m^6A_m as the substrate (*SI Appendix*, Fig. S14). We found that FTO^{WT} has the same demethylation activity for internal m^6A and m^6A_m in the same RNA sequence; the S229A mutation slightly decreases the m^6A demethylation activity of FTO (Fig. 3*D*). These results suggest that the substrate specificity of FTO primarily results from the interaction of residues in the catalytic pocket with the nucleobase N^6-methyladenine rather than the ribose ring; further, they support that S229 does likely form a weak H bond with 2′OH of m^6A.

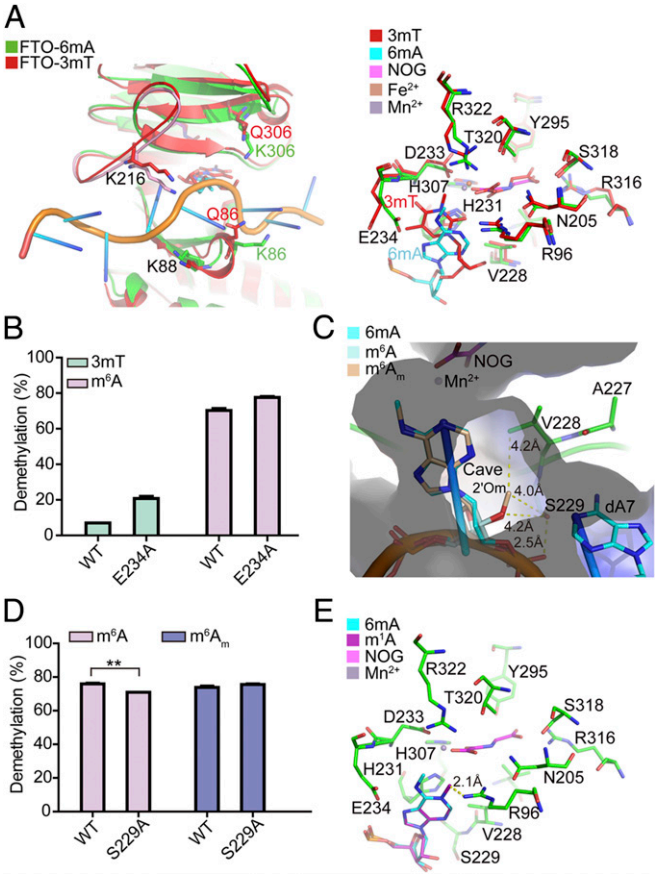

Fig. 3. Structural basis for substrate preference of FTO in the catalytic pocket. (*A*) Superposition of FTO-3mT nucleoside structure into the FTO-6mA structure. (*B*) Enzymatic activity comparison of WT and E234A mutation of FTO in catalyzing 3mT and m^6A for 1 h at 37 °C. m^6A-modified Oligo2 (10 μM) was incubated with 0.5 μM of WT or E234A mutation of FTO in 50 μL of reaction mixture (pH 7.0), while 3mT-modified Oligo1 (10 μM) was incubated with 10 μM of WT and E234A mutation of FTO in 50 μL of reaction mixture (pH 6.5). (*C*) Superposition of m^6A and m^6A_m nucleosides into the FTO-6mA structure. The electrostatic surface is shown. (*D*) Enzymatic activity comparison of 1 μM of WT and S229A mutation of FTO in catalyzing m^6A- and m^6A_m-modified Oligo3 (10 μM) for 15 min at 37 °C. (*E*) Superposition of the m^1A nucleoside into the FTO-6mA structure. Error bars indicate the mean ± SEM (n = 6, three biological replicates × two technical replicates), determined using an unpaired Student's t test. $^{**}P < 0.01$.

In addition to m^6A and m^6A_m, m^1A has also been reported as a substrate of FTO (32). The superposition of the m^1A nucleoside into the FTO-6mA structure suggests that the methyl group of m^1A would undergo significant clashes with R96 (Fig. 3*E*). Further, m^1A would have to rotate to facilitate catalysis, but steric hindrance with E234 on the opposite side of the catalytic pocket would likely interfere with such movement. Superposition of the FTO-6mA structure into the structure of AlkB–dsDNA with 1mA (AlkB-1mA; PDB ID code 3BI3) (34) confirmed this hypothesis. The structure showed that in the catalytic pocket of AlkB, the 1mA base rotates counterclockwise toward K134 (the corresponding residue of E234 in FTO) to avoid clashing with the side chain of M61 (the corresponding residue of R96 in FTO); meanwhile, the side chain of K134 flips ∼45° outward, generating enough space for 1mA base rotation (*SI Appendix*, Fig. S15). These observations revealed that the purine ring of m^1A loses H bonds with both E234 and R96 and the positively charged N1 is averse to the holding N^1-methyl group in the hydrophobic cave, explaining FTO's significantly lower enzymatic activity reported for m^1A/1mA compared with m^6A or 3mT (12, 32). Collectively, we demonstrated that N^6-methyladenine is the most favorable nucleobase substrate of FTO (*SI Appendix*, Fig. S16).

Consider our findings that FTO displays the same demethylation activity toward internal m^6A and m^6A_m positioned in the same RNA sequence (Fig. 3*D*) but that FTO has been shown to exhibit a preference for cap m^6A_m over internal m^6A in ssRNA (30). We found, upon superposition of an cap m^6A_m cap m^6A substrate into the FTO-6mA structure, that the m^7G cap can be accommodated in the large space next to pincer 2 (as expected) and that the m^7G nucleobase is in close contact with residue K86 from pincer 2 (Q86 in FTO^{WT}; *SI Appendix*, Fig. S17). We further examined whether residue Q86 would bind and recognize m^7G, and found that the mutation of Q86A or Q86L in FTO does not affect the cap m^6A_m demethylation activity in isolated mRNA in vitro (*SI Appendix*, Fig. S18). Thus, whether FTO provides a special residue to recognize the m^7G cap will remain a mystery until the complex structure of FTO bound to cap m^6A_m-modified RNA is solved. Moreover, the structure suggests that the large space next to pincer 2 can also accommodate other m^6A-modified RNAs with tertiary structures like stem loops. Our enzymatic activity assays showed that the sequence and the structure of RNAs indeed affect the demethylation activity of FTO (*SI Appendix*, Figs. S19 and S20). FTO exhibits twofold higher demethylation activity for m^6A positioned in a large stem loop compared with m^6A in a linear ssRNA (*SI Appendix*, Fig. S20).

Comparison of the Complex Structure of FTO Bound to 6mA-Modified ssDNA with Other AlkB Family Proteins. Multiple sequence alignment shows that AlkB family members share highly conserved active residues for catalysis, especially around the α-KG and Fe(II) binding sites (*SI Appendix*, Fig. S10). However, the structural conformation of the nucleic acid binding motifs varies a lot, for example, the unique loop (residues 210–223) and the short loop between β2 and β3 (residues 85–88) in FTO, where the two pincers are located. Our structure showed that the FTO unique loop is used for recognition of the sequence and structure of the RNA substrate (Figs. 2*B* and 4*A*); it interacts with the base of the RNA substrate through the key residue K216 and sterically prevents the binding of dsRNA and dsDNA (*SI Appendix*, Fig. S21). Notably, other AlkB family members (AlkB and ALKBH2) lose the corresponding motif of the FTO unique loop, explaining their capacity to take dsDNA as substrates for catalysis (*SI Appendix*, Fig. S21), while ALKBH5 and ALKBH8 prefer ssRNA due to the steric hindrance of a corresponding motif at this position. Specifically, ALKBH5 replaces the FTO unique loop with a short α-helix that prevents binding with dsRNA (Fig. 4*B*). Additionally, the other loop between β2 and β3 in FTO, where

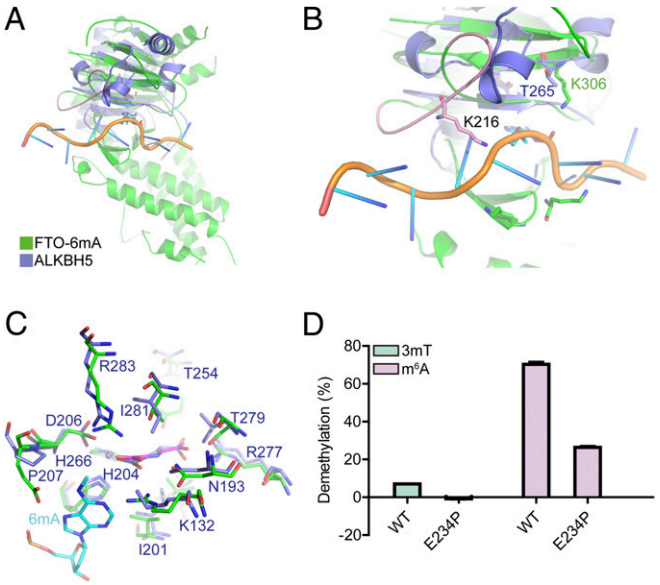

Fig. 4. Comparison of FTO and ALKBH5 in catalyzing m^6A. (*A*) Superposition of the ALKBH5 structure into the FTO-6mA structure. (*B*) The unique loop (pink) of FTO induces substrate selectivity variation between FTO and ALKBH5. (*C*) Superposition of the catalytic pocket of ALKBH5 with the FTO-6mA structure. (*D*) Enzymatic activity comparison of WT and the E234P mutation of FTO in catalyzing 3mT and m^6A for 1 h at 37 °C. The reaction condition is the same as in Fig. 3*D*. Error bars indicate the mean ± SEM ($n = 6$, three biological replicates × two technical replicates), determined using an unpaired Student's *t* test.

the two key residues K86 (Q86 in FTO^{WT}) and K88 are located, is significantly shorter than the corresponding loop in the other AlkB family members, further contributing to the unique nucleic acid substrate capacity of FTO.

Considering that in vitro biochemistry assays have shown that FTO exhibits higher enzyme kinetics efficiency with m^6A demethylation than does ALKBH5 (37, 38), we finally investigated the molecular mechanism for this kinetic difference. Sequence alignment and structural analysis suggest that E234 in human FTO is not conserved among human AlkB family members (*SI Appendix*, Fig. S10). The corresponding residue P207 in human ALKBH5 abolishes the hydrophilic interaction with N6 and N7 atoms of the 6mA purine ring (Fig. 4*C*). The mutation of E234P in FTO results in a 62% decrease in m^6A demethylation activity (Fig. 4*D*), confirming the functional contribution of E234 in substrate recognition and, importantly, explaining the significant lower m^6A demethylation activity (in vitro) reported for ALKBH5 compared with FTO (37, 38).

Discussion

To date, extensive efforts have been dedicated to identifying the physiological substrate(s) of FTO. It catalyzes the demethylation of m^6A and cap m^6A_m in mRNA, m^6A and m^6A_m in snRNA, and m^1A in tRNA (15, 30, 32). However, many questions remain unanswered, including how FTO recognizes such multiple-modification substrates, whether FTO displays a substrate preference, why FTO exhibits a preference for cap m^6A_m over internal m^6A in ssRNA, and why FTO has m^1A demethylation activity in tRNA or loop-structured RNA but no activity for linear ssRNA and ssDNA. Here we presented the structure of FTO bound to 6mA-modified ssDNA, which enabled us to investigate these mechanisms at the molecular level. The main conclusions from the biochemical assays and structural analysis described above include the following: (*i*) FTO prefers the methylated nucleobase N^6-methyladenine rather than 3mT and m^1A in the catalytic pocket. Residues R96 and E234 of FTO specifically interact

with the purine ring of N^6-methyladenine, and a hydrophobic cave holds the N^6-methyl group for demethylation. (*ii*) The demethylation activity of FTO is the same for internal m^6A and m^6A_m within the same RNA sequence, suggesting the binding interaction between the residues in FTO's catalytic pocket and the nucleobase N^6-methyladenine (rather than the structural differences of the ribose ring) plays the predominant role in mediating the enzymatic activity of FTO. (*iii*) The sequence and the tertiary structure of RNA can affect the enzymatic activity of FTO, which helps explain the activity preference of FTO for cap m^6A_m over internal m^6A in ssRNA and for m^1A in tRNA or loop-structured RNA over m^1A in linear ssRNA.

Here we demonstrated that the activity preference of FTO for cap m^6A_m over internal m^6A in ssRNA is because of the sequence and structure of RNA but not the differences of the ribose ring between m^6A_m and m^6A. The FTO-6mA structure showed that two pincers of FTO hold and bend the oligonucleotides for substrate demethylation. The feature of the cap structure (m^7Gppp) including the positively charged m^7G, the negatively charged triphosphate, and the 5′ terminus might increase the binding affinity with FTO and bend RNA easily for substrate demethylation. The subcellular localization of the FTO protein was found to affect its ability to perform different RNA modifications (32). Our FTO-6mA structure revealed that FTO does not accept dsRNA substrates but can accommodate ssRNA, RNA with tertiary structures like large stem loops, and cap structures. Therefore, the binding of FTO for various RNAs can further help define its targeted RNA modifications at specific RNAs. The m^6A reader domain YTH recognizes the N^6-methyl group through a hydrophobic cave (39); similarly, we also found FTO uses a hydrophobic cave for holding the N^6-methyl group for demethylation.

Both FTO and ALKBH5 mediate m^6A demethylation in mRNA (15, 37); however, they lead to completely different phenotypes: *FTO*-deficient mice have lean body mass and growth retardation, while *ALKBH5*-deficient male mice have impaired fertility (4, 5, 37). Apparently, FTO and ALKBH5 must take different RNAs as targets for demethylation, thereby leading to different phenotypes. Our structural analysis showed that FTO and ALKBH5 contain different structural conformations of the nucleic acid binding motifs, further confirming that they bind distinct RNA targets at molecular level.

Collectively, our biochemical and cellular results confirm that FTO demethylates both m^6A and cap m^6A_m in mRNA, thus providing a biochemical foundation for studying the mechanisms through which FTO is involved in biological processes and in human diseases. Moreover, our FTO-6mA structure provides a structural basis for understanding the mechanism of FTO-mediated m^6A, m^6A_m, and m^1A demethylation and will support the structure-guided design of selective inhibitors and/or activators for functional studies and potential therapeutic applications.

Materials and Methods

Experimental procedures for cloning, expression, and purification of wild-type and mutation FTO, knockdown of *FTO*, mRNA isolation, FTO demethylation activity assays, synthesis of the m^6A_m standard nucleoside and phosphoramidite, measurement of mRNA internal m^6A and cap m^6A_m levels using UPLC-MS/MS, oligonucleotide synthesis and purification, fluorescence anisotropy assay, measurement of 3mT, m^6A, and m^6A_m levels in oligonucleotides using HPLC, crystallization, data collection and structure determination, and statistical analysis are described in *SI Appendix, Supplementary Materials and Methods*.

ACKNOWLEDGMENTS. We thank the staff from beam line BL19U1 at the Shanghai Synchrotron Radiation Facility for assistance with crystal diffraction data collection. This work was supported by the National Basic Research Program of China (Grant 2017YFA0505201) and the National Natural Science Foundation of China (Grants 21722802, 21820102008, 21432002, and 21572133).

1. Peters T, Ausmeier K, Rüther U (1999) Cloning of Fatso (Fto), a novel gene deleted by the Fused toes (Ft) mouse mutation. *Mamm Genome* 10:983–986.
2. Dina C, et al. (2007) Variation in FTO contributes to childhood obesity and severe adult obesity. *Nat Genet* 39:724–726.
3. Frayling TM, et al. (2007) A common variant in the FTO gene is associated with body mass index and predisposes to childhood and adult obesity. *Science* 316:889–894.
4. Fischer J, et al. (2009) Inactivation of the Fto gene protects from obesity. *Nature* 458: 894–898.
5. Church C, et al. (2010) Overexpression of Fto leads to increased food intake and results in obesity. *Nat Genet* 42:1086–1092.
6. Kaklamani V, et al. (2011) The role of the fat mass and obesity associated gene (FTO) in breast cancer risk. *BMC Med Genet* 12:52.
7. Hernández-Caballero ME, Sierra-Ramírez JA (2015) Single nucleotide polymorphisms of the FTO gene and cancer risk: An overview. *Mol Biol Rep* 42:699–704.
8. Fawcett KA, Barroso I (2010) The genetics of obesity: FTO leads the way. *Trends Genet* 26:266–274.
9. Kim YJ, et al. (2016) Association of metabolites with obesity and type 2 diabetes based on FTO genotype. *PLoS One* 11:e0156612.
10. Keller L, et al. (2011) The obesity related gene, FTO, interacts with APOE, and is associated with Alzheimer's disease risk: A prospective cohort study. *J Alzheimers Dis* 23:461–469.
11. Wang L, Shen H, Liu H, Guo G (2015) Mixture SNPs effect on phenotype in genome-wide association studies. *BMC Genomics* 16:3.
12. Gerken T, et al. (2007) The obesity-associated FTO gene encodes a 2-oxoglutarate-dependent nucleic acid demethylase. *Science* 318:1469–1472.
13. Jia G, et al. (2008) Oxidative demethylation of 3-methylthymine and 3-methyluracil in single-stranded DNA and RNA by mouse and human FTO. *FEBS Lett* 582:3313–3319.
14. Han Z, et al. (2010) Crystal structure of the FTO protein reveals basis for its substrate specificity. *Nature* 464:1205–1209.
15. Jia G, et al. (2011) N6-methyladenosine in nuclear RNA is a major substrate of the obesity-associated FTO. *Nat Chem Biol* 7:885–887.
16. Fu Y, et al. (2013) FTO-mediated formation of N^6-hydroxymethyladenosine and N^6-formyladenosine in mammalian RNA. *Nat Commun* 4:1798.
17. Fustin JM, et al. (2013) RNA-methylation-dependent RNA processing controls the speed of the circadian clock. *Cell* 155:793–806.
18. Geula S, et al. (2015) Stem cells. m6A mRNA methylation facilitates resolution of naïve pluripotency toward differentiation. *Science* 347:1002–1006.
19. Haussmann IU, et al. (2016) m^6A potentiates Sxl alternative pre-mRNA splicing for robust Drosophila sex determination. *Nature* 540:301–304.
20. Li HB, et al. (2017) m^6A mRNA methylation controls T cell homeostasis by targeting the IL-7/STAT5/SOCS pathways. *Nature* 548:338–342.
21. Hess ME, et al. (2013) The fat mass and obesity associated gene (Fto) regulates activity of the dopaminergic midbrain circuitry. *Nat Neurosci* 16:1042–1048.
22. Zhao X, et al. (2014) FTO-dependent demethylation of N6-methyladenosine regulates mRNA splicing and is required for adipogenesis. *Cell Res* 24:1403–1419.
23. Zhou J, et al. (2015) Dynamic m(6)A mRNA methylation directs translational control of heat shock response. *Nature* 526:591–594.
24. Xiang Y, et al. (2017) RNA m^6A methylation regulates the ultraviolet-induced DNA damage response. *Nature* 543:573–576.
25. Li Z, et al. (2017) FTO plays an oncogenic role in acute myeloid leukemia as a N^6-methyladenosine RNA demethylase. *Cancer Cell* 31:127–141.
26. Fu Y (2012) Dynamic regulation of RNA modifications by AlkB family dioxygenases. PhD thesis (Univ of Chicago, Chicago).
27. Dominissini D, et al. (2012) Topology of the human and mouse m^6A RNA methylomes revealed by m6A-seq. *Nature* 485:201–206.
28. Linder B, et al. (2015) Single-nucleotide-resolution mapping of m6A and m6Am throughout the transcriptome. *Nat Methods* 12:767–772.
29. Molinie B, et al. (2016) m(6)A-LAIC-seq reveals the census and complexity of the m(6)A epitranscriptome. *Nat Methods* 13:692–698.
30. Mauer J, et al. (2017) Reversible methylation of m^6A_m in the 5′ cap controls mRNA stability. *Nature* 541:371–375.
31. Akichika S, et al. (2018) Cap-specific terminal N^6-methylation of RNA by an RNA polymerase II-associated methyltransferase. *Science* 363:eaav0080.
32. Wei J, et al. (2018) Differential m^6A, m^6A_m, and m^1A demethylation mediated by FTO in the cell nucleus and cytoplasm. *Mol Cell* 71:973–985.e5.
33. Mishina Y, Chen LX, He C (2004) Preparation and characterization of the native iron (II)-containing DNA repair AlkB protein directly from Escherichia coli. *J Am Chem Soc* 126:16930–16936.
34. Yang CG, et al. (2008) Crystal structures of DNA/RNA repair enzymes AlkB and ABH2 bound to dsDNA. *Nature* 452:961–965.
35. Holland PJ, Hollis T (2010) Structural and mutational analysis of Escherichia coli AlkB provides insight into substrate specificity and DNA damage searching. *PLoS One* 5: e8680.
36. Owen B, McMurray C (2009) Rapid method for measuring DNA binding to protein using fluorescence anisotropy. *Protoc Exch*, 10.1038/nprot.2009.80.
37. Zheng G, et al. (2013) ALKBH5 is a mammalian RNA demethylase that impacts RNA metabolism and mouse fertility. *Mol Cell* 49:18–29.
38. Zou S, et al. (2016) N(6)-methyladenosine: A conformational marker that regulates the substrate specificity of human demethylases FTO and ALKBH5. *Sci Rep* 6:25677.
39. Xu C, et al. (2014) Structural basis for selective binding of m^6A RNA by the YTHDC1 YTH domain. *Nat Chem Biol* 10:927–929.